High-order above-threshold ionization beyond the first-order Born approximation

A. Čerkić,[1] E. Hasović,[1] D. B. Milošević,[1,2] and W. Becker[2]
[1]*Faculty of Science, University of Sarajevo, Zmaja od Bosne 35, 71000 Sarajevo, Bosnia and Herzegovina*
[2]*Max-Born-Institut, Max-Born-Str. 2a, 12489 Berlin, Germany*
(Received 11 December 2008; published 23 March 2009)

In the improved strong-field approximation, which describes high-order above-threshold ionization (HATI), the rescattering of the ionized electron on the parent ion is described within the first-order Born approximation. The low-frequency approximation for laser-assisted scattering goes beyond the first Born approximation. In the present paper, we derive the low-frequency approximation for HATI. The rescattering amplitude in the first Born approximation is replaced by the exact scattering amplitude calculated on the energy shell. Our numerical results for the angle-resolved HATI energy spectra show that the difference between the improved strong-field approximation and the low-frequency approximation is significant for scattering away from the laser polarization axis. In the context of quantum-orbit theory and the uniform approximation, we also show that on the back-rescattering ridge, the rescattering T-matrix element can be factorized into the product of the incoming flux and the elastic-scattering cross section so that the latter can be extracted from the angle- and energy-resolved HATI spectra.

DOI: 10.1103/PhysRevA.79.033413 PACS number(s): 42.50.Hz, 34.50.Rk, 32.80.Rm, 32.80.Qk

I. INTRODUCTION

High-order above-threshold ionization (HATI) of atoms and molecules by an intense laser field is a nonperturbative quantum-mechanical phenomenon where the ionized electron absorbs many more photons than the minimum number necessary for ionization. The electron energy spectra of this process are characterized by three regions. The low-energy part of the spectra extends up to $(3-4)U_p$, with U_p the electron's ponderomotive energy in the laser field, and decreases exponentially with increasing energy. It is followed by a plateau where the ionization yield is almost independent of the electron energy. The plateau finishes with a cutoff at $10U_p$. The low-energy electrons are called the direct electrons since after ionization they are not affected anymore by the atomic binding potential and go directly to the detector. In the present paper we will be interested in the high-energy electrons, which acquire their high energy from the laser field after they have been rescattered off the binding potential. To be specific, the ionized electron is accelerated by the laser field and may revisit its parent ion, having a kinetic energy of up to $3.17U_p$. This electron may backscatter off the ion and again be accelerated by the laser field reaching a kinetic energy of up to $10U_p$ (this explains the $10U_p$ cutoff law). The rescattered electrons form the above-mentioned plateau whose yield is lower by several orders of magnitude than the yield of direct electrons. The number of publications devoted to the HATI process is large. We will be contented with mentioning the review articles [1–4].

Recently, with the development of attosecond science [4–7], the HATI process has attracted more attention. Namely, HATI induced by femtosecond infrared lasers unfolds on the subfemtosecond time scale. Furthermore, the effective current density of the returning electrons is much higher than that of electron beams from conventional laboratory electron sources [7,8]. Therefore, the HATI electrons can be used to study atomic and molecular structures as well as to follow and control chemical and biological reactions which develop on this time scale. The possibility to use laser-induced electron-diffraction spectra for imaging molecules was suggested in [9] (see also [10–12] and the recent review [13]).

Present computer facilities allow one to study *ab initio* only the very simplest systems such as He and H_2^+. HATI of more complex atomic and molecular systems is studied by solving the time-dependent Schrödinger equation within the single-active electron approximation using carefully chosen effective potentials. Even these calculations are time consuming and not adequate for the simulation of real experiments. Models, such as the above-mentioned three-step model, and approximate theories are more suitable for this purpose. Furthermore, from such theories the physics of atomic and molecular processes in strong fields can be better understood. Arguably, the strong-field approximation (SFA) is the most successful theory of this kind. It was originally formulated for the direct electrons [14]. Once the electron has entered the continuum it is assumed only to feel the laser field and not the atomic or molecular binding potential. It is then described by the so-called Volkov state (the state of a free electron in the laser field which is known in analytical form). Later on, the SFA theory was generalized to approximately include the interaction with the binding potential. This has been done in the fashion of a Born series whose zeroth-order term yields the direct above-threshold ionization, while the terms of the first order in the binding potential enable rescattering. This is the so-called improved SFA (ISFA). Its various versions were presented in [15–19] (see also the review articles [2–4] and the more recent Refs. [20–23]; the name SFA2 was suggested in [24]). The ISFA for molecular systems was recently introduced in [11].

It is clear that the ISFA can only be trusted to the extent that the first-order Born approximation (1BA), on which it is built, is reliable. This depends on the energy of the rescattering electron and the shape of the scattering potential. The 1BA is exact for a Coulomb potential but not in general. Especially, it is not exact if the potential includes a short-

range contribution, as is the case for optimized effective one-electron potentials. Hence, if we want to "improve" the ISFA we have to go beyond the first Born approximation for the laser-assisted rescattering in the third step of HATI. Such a procedure was suggested by Lin and co-workers [25,26]. They introduced the concept of the back-rescattering ridge (BRR; see also [24]) in the momentum spectrum. The BRR is formed by those electrons that return to their parent ion with close to maximal kinetic energy (approximately $3.17U_p$) and are rescattered into the backward cone. By comparison to numerical solutions of the time-dependent Schrödinger equation, Lin and co-workers [25,26] showed that the yield of photoelectrons with momentum $\mathbf{p}$ can be represented as the product of the elastic differential cross section $\sigma(p_r,\theta_r)$ for scattering of a free electron with energy $p_r^2/2$ by the scattering angle θ_r, and the factor $F(p_r)$ which describes the flux of the returning electron wave packet with momentum near p_r (it was shown that it does not depend on θ_r for $\theta_r > 120°$),

$$R(\mathbf{p}) = F(p_r)\sigma(p_r,\theta_r). \tag{1}$$

Here $\mathbf{p}=\mathbf{p}_r-\mathbf{A}_r$ is the momentum at the detector, with $\mathbf{A}_r \equiv \mathbf{A}(t_r)$ the vector potential of the laser field at the time of rescattering, and $p_r=\sqrt{3.17/2}A_{\max}=1.26A_{\max}$, where $A_{\max}$ is the amplitude of the vector potential. In Refs. [25,26], the factorization property (1) was presented as a plausible conjecture and no theoretical derivation from the HATI transition amplitude was given. Nevertheless, this approach was successfully used to extract the differential cross section for elastic electron scattering off positive ions of inert gases from the experimental HATI data in Refs. [27,28].

In the present paper we will derive a SFA-type theory that goes beyond the ISFA. Laser-assisted potential scattering was treated within the 1BA in Ref. [29]. A step further is to treat the laser-assisted scattering using the so-called low-frequency approximation (LFA) which includes the 1BA as a special case. The LFA for laser-assisted electron-atom scattering was introduced by Kroll and Watson [30]. More details can be found in the book [31] and in the review article [32]. We will use the so-called off-shell LFA [33,34], which can be approximated by the on-shell LFA [35,36].

We introduce our theory in Sec. II. We first review the improved SFA theory in order to introduce the notation. Our low-frequency approximation for HATI is given in Sec. II B (details of the derivation are relegated to Appendix A). In Sec. II C we will derive, using the LFA and quantum-orbit theory, the factorization property (1) for the rescattering matrix element along the BRR. In Sec. II D we present the details of the (re)scattering geometry and estimate the maximal electron momenta and energies. Section III contains our numerical results. Finally, our conclusions are given in Sec. IV. We will use the atomic system of units ($\hbar=e=m=4\pi\varepsilon_0=1$).

II. THEORY

A. Improved strong-field approximation

Our starting point is the transition matrix element from the initial bound state $|\psi_i(t')\rangle$ to the final state $|\psi_{\mathbf{p}}(t)\rangle$ of the electron having the asymptotic momentum $\mathbf{p}$

$$M_{\mathbf{p}i}(t,t') = \langle\psi_{\mathbf{p}}(t)|U(t,t')|\psi_i(t')\rangle. \tag{2}$$

The total time-evolution operator $U(t,t')$ of the Hamiltonian $H(t)=H_0+V_L(t)+V(\mathbf{r})$, $H_0=-\boldsymbol{\nabla}^2/2$, $\boldsymbol{\nabla}\equiv\partial/\partial\mathbf{r}$, satisfies the Dyson equations

$$U(t,t') = U_V(t,t') - i\int_{t'}^{t} d\tau U(t,\tau)V_L(\tau)U_V(\tau,t'), \tag{3}$$

$$U(t,\tau) = U_L(t,\tau) - i\int_{\tau}^{t} d\tau' U(t,\tau')V(\mathbf{r})U_L(\tau',\tau). \tag{4}$$

The evolution operator U_V (U_L) corresponds to the Hamiltonian $H_V=H_0+V$ ($H_L=H_0+V_L$), where $V_L(t)$ is the laser-field–electron interaction, while $V(\mathbf{r})=V_C(r)+V_S(r)$, where $V_C(r)=-Z/r$ is the Coulomb interaction and $V_S(r)$ is a short-range interaction. If the laser-field–electron interaction is chosen in length gauge and dipole approximation, $V_L(t)=\mathbf{r}\cdot\mathbf{E}(t)$, with $\mathbf{E}(t)=-d\mathbf{A}(t)/dt$ the electric field vector, then the Volkov time-evolution operator is given by

$$U_L(t,t') = \int d^3\mathbf{k}|\chi_{\mathbf{k}}(t)\rangle\langle\chi_{\mathbf{k}}(t')|, \tag{5}$$

$$|\chi_{\mathbf{k}}(t)\rangle = |\mathbf{k}+\mathbf{A}(t)\rangle\exp[-iS_{\mathbf{k}}(t)], \tag{6}$$

$$\frac{dS_{\mathbf{k}}(t)}{dt} = \frac{1}{2}[\mathbf{k}+\mathbf{A}(t)]^2, \tag{7}$$

where $|\mathbf{q}\rangle$ denotes a plane-wave state $\langle\mathbf{r}|\mathbf{q}\rangle=(2\pi)^{-3/2}\exp(i\mathbf{q}\cdot\mathbf{r})$.

We consider an ionization process in which the interaction with the laser field is turned off at the times t and t' so that the states $|\psi_i(t')\rangle=|\psi_i\rangle e^{-iE_it'}$ and $|\psi_{\mathbf{p}}(t)\rangle=|\psi_{\mathbf{p}}\rangle e^{-iE_{\mathbf{p}}t}$ are mutually orthogonal eigenstates of the Hamiltonian H_V with the eigenenergies $E_i<0$ (atomic binding energy) and $E_{\mathbf{p}}=\mathbf{p}^2/2$, respectively. Introducing Eq. (3) into Eq. (2) and replacing in the resulting equation the operator $U(t,\tau)$ with Eq. (4), we get

$$M_{\mathbf{p}i}(t,t') = M_{\mathbf{p}i}^{(0)}(t,t') + M_{\mathbf{p}i}^{(1)}(t,t'), \tag{8}$$

$$M_{\mathbf{p}i}^{(0)}(t,t') = -i\int_{t'}^{t} d\tau\langle\psi_{\mathbf{p}}(t)|U_L(t,\tau)V_L(\tau)|\psi_i(\tau)\rangle, \tag{9}$$

$$M_{\mathbf{p}i}^{(1)}(t,t') = (-i)^2\int_{t'}^{t} d\tau\int_{\tau}^{t} d\tau'\langle\psi_{\mathbf{p}}(t)|U(t,\tau') \times V(\mathbf{r})U_L(\tau',\tau)V_L(\tau)|\psi_i(\tau)\rangle. \tag{10}$$

By now no approximation has been made. If in Eq. (9) we approximate $\langle\psi_{\mathbf{p}}(t)|U_L(t,\tau)$ with $\langle\chi_{\mathbf{p}}(\tau)|$, i.e., with the Volkov state that corresponds to the electron having the asymptotic momentum $\mathbf{p}$ outside the laser field, we obtain the standard direct SFA in its length gauge version [14]

$$M_{\mathbf{p}i}^{\mathrm{SFA}(0)} \equiv M_{\mathbf{p}i}^{(0)}(\infty,-\infty), \tag{11}$$

$$M_{\mathbf{p}i}^{(0)}(t,t') = \int_{t'}^{t} d\tau\mathcal{M}_{\mathbf{p}i}^{(0)}(\tau), \tag{12}$$

$$\mathcal{M}_{\mathbf{p}i}^{(0)}(\tau) = -i\langle\chi_{\mathbf{p}}(\tau)|\mathbf{r}\cdot\mathbf{E}(\tau)|\psi_i(\tau)\rangle. \tag{13}$$

Using this notation and Eq. (5) we can write

$$M_{\mathbf{p}i}^{(1)}(t,t') = \int_{t'}^{t} d\tau \int d^3\mathbf{k}\mathcal{M}_{\mathbf{k}i}^{(0)}(\tau)M_{\mathbf{pk}}(t,\tau), \tag{14}$$

with

$$M_{\mathbf{pk}}(t,\tau) = -i\int_{\tau}^{t} d\tau'\langle\psi_{\mathbf{p}}(t)|U(t,\tau')V(\mathbf{r})|\chi_{\mathbf{k}}(\tau')\rangle. \tag{15}$$

If we replace in Eq. (15) $\langle\psi_{\mathbf{p}}(t)|U(t,\tau')$ with $\langle\chi_{\mathbf{p}}(\tau')|$, we obtain the ISFA mentioned in Sec. I

$$M_{\mathbf{p}i}^{\mathrm{ISFA}} = M_{\mathbf{p}i}^{\mathrm{SFA}(0)} + M_{\mathbf{p}i}^{\mathrm{SFA}(1)}(\infty,-\infty), \tag{16}$$

with

$$M_{\mathbf{p}i}^{\mathrm{SFA}(1)}(t,t') \equiv \int_{t'}^{t} d\tau \int d^3\mathbf{k}\mathcal{M}_{\mathbf{k}i}^{(0)}(\tau)\int_{\tau}^{t} d\tau'\mathcal{M}_{\mathbf{pk}}^{(0)}(\tau'), \tag{17}$$

where

$$\mathcal{M}_{\mathbf{pk}}^{(0)}(\tau') = -i\langle\chi_{\mathbf{p}}(\tau')|V(\mathbf{r})|\chi_{\mathbf{k}}(\tau')\rangle \tag{18}$$

is the amplitude for the laser-assisted scattering in the first Born approximation [29]. The term $M_{\mathbf{p}i}^{\mathrm{SFA}(1)}(t,t')$ is the rescattering amplitude, which is responsible for the high-energy plateau in the electron energy spectrum. This amplitude incorporates the three-step model of HATI: the electron is ionized at the time τ, accelerates under the influence of only the laser field until the time τ', when the electron, being in the Volkov state with the momentum $\mathbf{k}$, (re)scatters elastically off the potential $V(\mathbf{r})$, and reaches the detector having the final momentum $\mathbf{p}$ outside the laser field.

B. Low-frequency approximation

In the present paper we want to go one step further and to include the rescattering effects beyond the 1BA (18). To this end, it is suggestive to make the replacement

$$\mathcal{M}_{\mathbf{pk}}^{(0)}(\tau') \to \mathcal{M}_{\mathbf{pk}}^{\mathrm{LFA}}(\tau') \equiv -i\langle\chi_{\mathbf{p}}(\tau')|T_V(E_{\mathbf{p}+\mathbf{A}(\tau')})|\chi_{\mathbf{k}}(\tau')\rangle. \tag{19}$$

Here,

$$T_V(E) = V + VG_V(E)V \tag{20}$$

is the exact T matrix for elastic scattering at the energy E off the potential $V(\mathbf{r})$, and

$$G_V(E) = (E + i\varepsilon - H_V)^{-1}, \quad \varepsilon \to 0^+ \tag{21}$$

is the stationary Green's operator in the absence of the laser field.

The new expression (19) describes scattering of a Volkov electron incident with drift momentum $\mathbf{k}$ [velocity $\mathbf{v}(\tau') \equiv \mathbf{k}+\mathbf{A}(\tau')$ at the time of collision] into a final Volkov state with drift momentum $\mathbf{p}$. Therein, the interactions of the electron with the scattering potential and with the laser field are well separated. First, the electron interacts with the laser field but not the potential, then the laser field is turned off while the electron interacts with the potential and changes its drift momentum from $\mathbf{k}$ to $\mathbf{p}$, and finally again the electron propagates in the presence of just the laser field. This approximation to the full time-dependent dynamics should be justified if the laser-driven velocity changes only little while the electron passes over a distance of the order of the range of the potential. This is particularly well satisfied for comparably high energy and long laser wavelength. The right-hand side of Eq. (19) can be re-expressed in terms of the stationary solution $|\psi_{\mathbf{p}+\mathbf{A}(\tau')}\rangle$ of the Hamiltonian H_V so that

$$\langle\chi_{\mathbf{p}}(\tau')|T_V(E_{\mathbf{p}+\mathbf{A}(\tau')})|\chi_{\mathbf{k}}(\tau')\rangle = e^{iS_{\mathbf{p}}(\tau')}\langle\psi_{\mathbf{p}+\mathbf{A}(\tau')}|V(\mathbf{r})|\chi_{\mathbf{k}}(\tau')\rangle. \tag{22}$$

A more rigorous derivation of Eqs. (19) and (22) can be found in Appendix A.

For a periodic laser field with the period $T=2\pi/\omega$, the transition amplitude can be decomposed in the form [3,21]

$$M_{\mathbf{p}i}^{\mathrm{SFA}(j)} = -2\pi i\sum_n \delta(E_{\mathbf{p}} - E_i + U_p - n\omega)T_{\mathbf{p}i}^{\mathrm{SFA}(j)}(n), \tag{23}$$

where $T_{\mathbf{p}i}^{\mathrm{SFA}(j)}(n)$, $j=0,1$, is the corresponding T-matrix element of the above-threshold ionization process. The argument of the δ function displays energy conservation and U_p is the ponderomotive energy defined by the nonperiodic part of $\frac{1}{2}\int^t dt'\mathbf{A}^2(t') = \mathcal{U}_1(t) + U_p t$, with $\mathcal{U}_1(t+T)=\mathcal{U}_1(t)$. For more details and the choice of the ground-state wave function ψ_i for the inert gases He, Ne, Ar, Kr, and Xe, and the negative ions H^-, F^-, Cl^-, Br^-, and I^-, see Refs. [20,19], respectively. A similar expression can be obtained for the off-shell LFA transition amplitudes. In this case, the corresponding T-matrix element is given by

$$T_{\mathbf{p}i}^{\mathrm{LFA}(1)}(n) = i\int_0^T \frac{d\tau}{T}\int d^3\mathbf{k}\int_{\tau}^{\infty} d\tau'\mathcal{M}_{\mathbf{pk}}^{\mathrm{LFA}}(\tau')\mathcal{M}_{\mathbf{k}i}^{(0)}(\tau). \tag{24}$$

Finally, the differential ionization rate with absorption of n photons in the LFA is given by

$$w_{\mathbf{p}i}^{\mathrm{LFA}}(n) = 2\pi p|T_{\mathbf{p}i}^{\mathrm{SFA}(0)}(n) + T_{\mathbf{p}i}^{\mathrm{LFA}(1)}(n)|^2. \tag{25}$$

The five-dimensional integral over τ, τ', and $\mathbf{k}$ in Eq. (24) can be solved numerically. This gives our off-shell LFA, or shortly LFA, for the rescattering matrix element. However, we will normally use the saddle-point approximation for the evaluation of the five-dimensional integral. The terms in the exponent in the T-matrix element (24) can be combined into the action

$$\mathcal{S}(\tau,\tau',\mathbf{k}) = S_{\mathbf{p}}(\tau') - S_{\mathbf{k}}(\tau') + S_{\mathbf{k}}(\tau) - E_i\tau, \tag{26}$$

with the partial actions defined in Eq. (7). The integral over time τ' in Eq. (15) gives the largest contribution if the action is stationary, i.e., if $\partial\mathcal{S}/\partial\tau'=0$. This stationarity condition leads to the following equation for the rescattering time τ':

$$\frac{1}{2}[\mathbf{p}+\mathbf{A}(\tau')]^2=\frac{1}{2}[\mathbf{k}+\mathbf{A}(\tau')]^2. \tag{27}$$

This means that (re)scattering at the time τ' is elastic: the electron energy in the laser field at the time τ' is equal before and after scattering. Equation (A6) with the condition (27) is the analog of the on-shell LFA in laser-assisted potential scattering [33–36]. The corresponding on-shell LFA for HATI is obtained by solving the integral over the rescattering time τ' using the saddle-point method. The result is

$$T^{\mathrm{LFA}(1)}_{\mathbf{p}i,\mathrm{on}}(n)=-i\int_0^T\frac{d\tau}{T}\int d^3\mathbf{k}\sum_{\tau'_r}\sqrt{\frac{2\pi i}{(\mathbf{k}-\mathbf{p})\cdot\mathbf{E}(\tau'_r)}}$$
$$\times\langle\psi_{\mathbf{p}+\mathbf{A}(\tau'_r)}|V(\mathbf{r})|\mathbf{k}+\mathbf{A}(\tau'_r)\rangle$$
$$\times\langle\mathbf{k}+\mathbf{A}(\tau)|\mathbf{r}\cdot\mathbf{E}(\tau)|\psi_i\rangle e^{i\mathcal{S}(\tau,\tau'_r,\mathbf{k})}, \tag{28}$$

where the saddle-point solutions for the time of rescattering τ'_r satisfy Eq. (27). The result (28) is our on-shell LFA for the rescattering T-matrix element.

The off-shell and on-shell LFAs for electron-atom scattering were considered in Ref. [33] using the [1,1] Padé approximation, for which the matrix elements are given in analytical form. For the on-shell LFA, one can also use numerical solutions for the elastic-scattering amplitude, taking into account that $\psi_{\mathbf{p}}$ is the solution of the stationary Schrödinger equation $H_V\psi_{\mathbf{p}}=E_{\mathbf{p}}\psi_{\mathbf{p}}$. As we have mentioned, a similar procedure was realized in Refs. [25,26]. In Appendix B, we present a method for the calculation of the scattering amplitude.

C. Saddle-point method and the factorization formula for the rescattering matrix element along the BRR

Application of the saddle-point method to the five-dimensional integral in Eq. (24) (see the review articles [2,4] for its standard [2] and modified [4] versions) yields

$$T^{\mathrm{LFA}(1)}_{\mathbf{p}i,\mathrm{SPM}}(n)=\sum_s\langle\psi_{\mathbf{p}+\mathbf{A}(\tau'_s)}|V(\mathbf{r})|\mathbf{k}_s+\mathbf{A}(\tau'_s)\rangle$$
$$\times\mathcal{A}(\tau_s,\tau'_s,\mathbf{k}_s)e^{i\mathcal{S}(\tau_s,\tau'_s,\mathbf{k}_s)}, \tag{29}$$

where we have explicitly separated the rescattering part of the amplitude, denoting the remaining part by $\mathcal{A}(\tau_s,\tau'_s,\mathbf{k}_s)$. The saddle-point solutions, labeled by the index s, are simultaneous solutions of the system of equations $\partial\mathcal{S}/\partial\tau=0$, $\partial\mathcal{S}/\partial\tau'=0$, and $\partial\mathcal{S}/\partial\mathbf{k}=\mathbf{0}$. The classification of these solutions, in the context of quantum-orbit theory, is given in Ref. [21] by the multi-index $s\equiv\{\alpha\beta m\}$, $\alpha=\pm1$, $\beta=\pm1$, $m=0,1,2,\ldots$. For each electron emission angle θ, near the cutoff energy two solutions of one pair $\alpha=\pm1$ approach each other very closely. The highest cutoff energy corresponds to $\beta=-1$ and $m=0$ and is well separated from the closest $\beta m=-11$ cutoff. This is valid for all scattering angles θ (see Fig. 4 in [21]). For example, for Xe atoms ($E_i=-12.13$ eV) at the laser intensity 1.5×10^{14} W/cm^2 and wavelength 760 nm, we have $E_{\mathbf{p},\max}(\theta=0;\beta m=-10)=10.76U_p$, while $E_{\mathbf{p},\max}(\theta=0;\beta m=-11)=9.03U_p$. For $\theta=0$, all solutions with $\beta=+1$ have their cutoff energies below $8U_p$, while the other solutions for $\beta=-1$ have their cutoff between $8U_p$ and $9.03U_p$. For the cutoff at $\theta=0$ the approximate semiclassical analytical formula [37] $E_{\mathbf{p},\max}(\theta=0)=10.007U_p-0.538E_i$ is valid. For the above Xe example we obtain $E_{\mathbf{p},\max}(\theta=0)=10.81U_p$ which is very close to the value of $10.76U_p$ obtained numerically.

The above result is important in the context of the BRR. Namely, for $E_{\mathbf{p}}(\theta)>E_{\mathbf{p},\max}(\theta;\beta m=-11)$ only the two solutions $s_1=\{+1-10\}$ and $s_2=\{-1-10\}$ contribute to the sum in (29). Near the cutoff, the shorter-orbit ($\alpha=+1$) and the longer-orbit ($\alpha=-1$) solutions merge into one (described by the uniform approximation in [21]). Therefore, for high-energy electrons along the BRR the rescattering matrix element can be factorized as

$$T^{\mathrm{BRR}}_{\mathbf{p}i}(n)=-(2\pi)^{-2}f(p_s,\theta_s)\mathcal{A}_s e^{i\phi_s+i\varphi_p(\tau'_s)}, \tag{30}$$

where $\mathcal{A}_s\equiv\mathcal{A}(\tau_s,\tau'_s,\mathbf{k}_s)$, $\phi_s\equiv S_{\mathbf{k}_s}(\tau_s)-E_i\tau_s-E_{\mathbf{k}_s}(\omega\tau'_s-\tan\omega\tau'_s)/\omega$, $\varphi_p(\tau'_s)=E_{\mathbf{p}}(\omega\tau'_s-\tan\omega\tau'_s)/\omega$, $s\equiv s(\beta m=-10)$, and $f(p_s,\theta_s)$ is the scattering amplitude for elastic scattering of a free electron with energy $p_s^2/2=(\mathbf{p}+\mathbf{A}_s)^2/2=(\mathbf{k}_s+\mathbf{A}_s)^2/2$ into the scattering angle θ_s by the ion described by the potential $V(\mathbf{r})$ (see Appendix B). Here $\mathbf{A}_s\equiv\mathbf{A}(\tau'_s)$ is the vector potential at the time τ'_s where the two solutions s_1 and s_2 merge. This time, together with the corresponding value of $E_{\mathbf{p},\max}(\theta;\beta m=-10)$, can be determined using the method described in Ref. [21]. In Eq. (30) we have explicitly separated the phase $\varphi_p(\tau'_s)$ (note that its imaginary part is small since $\mathrm{Im}\,\tau'_s\ll\mathrm{Re}\,\tau'_s$), which changes quickly with the momentum p since $E_{\mathbf{p}}/\omega$ is large. The amplitude $\mathcal{A}_s$ and the remaining phase ϕ_s depend only slowly on the momentum p and the angle θ, since the saddle-point solutions change only slightly near the corresponding cutoff. From Eqs. (29) and (30) it follows that the rescattering differential ionization rate takes the form

$$w^{\mathrm{BRR}}_{\mathbf{p}i}(n)\approx\frac{p}{(2\pi)^3}|\mathcal{A}_s e^{i\phi_s}|^2\sigma(p_s,\theta_s), \tag{31}$$

where

$$\sigma(p_s,\theta_s)=|f(p_s,\theta_s)|^2=(2\pi)^4|\langle\psi_{\mathbf{p}+\mathbf{A}_s}|V(\mathbf{r})|\mathbf{k}_s+\mathbf{A}_s\rangle|^2 \tag{32}$$

is the differential cross section which corresponds to the amplitude $f(p_s,\theta_s)$. Equation (32) allows us to extract the differential cross section from the observed HATI spectrum (see the examples in Sec. III). Furthermore, using Eq. (30) for the phase of the scattering amplitude we obtain

$$\arg f(p_s,\theta_s)=\arg T^{\mathrm{BRR}}_{\mathbf{p}i}(n)-\varphi_p(\tau'_s), \tag{33}$$

where we have neglected the phase of $\mathcal{A}_s e^{i\phi_s}$ since it contributes only as a constant. Therefore, knowing the saddle-point solutions along the BRR we can also determine the phase of the elastic-scattering amplitude provided we know the phase of the rescattering T-matrix element. Unfortunately, the latter cannot be retrieved from experimental HATI data. Hence, we will only use the phase relation (33) as a consistency check. This will also be illustrated in Sec. III.

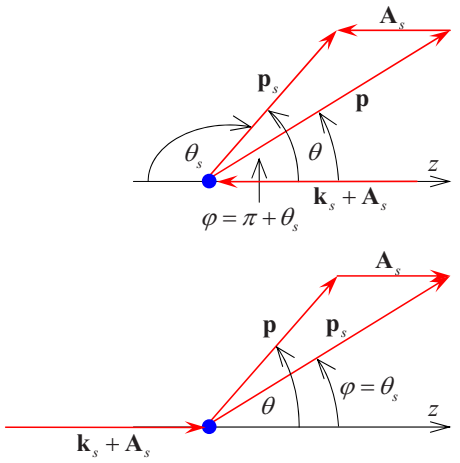

FIG. 1. (Color online) Two possible geometries of the (re)scattering event. For negative values of k_s+A_s (upper panel) the scattering and laboratory systems have opposite z axis so that $\theta_s=\varphi-\pi$. For the lower panel these systems overlap so that $\theta_s=\varphi$.

D. Geometry of (re)scattering and estimate of the maximal electron momenta

We suppose that the laser polarization is along the z axis, $\hat{\mathbf{e}}_L=\hat{\mathbf{z}}$, and that the rescattering takes place in the zx plane. The final (drift) electron momentum at the detector is $\mathbf{p}=(p_z,p_x)=(p\cos\theta, p\sin\theta)$, while the electron momentum immediately after the rescattering is $\mathbf{p}_s=(p_s\cos\varphi, p_s\sin\varphi)$. The ratio of the z component and the x component of the relation $\mathbf{p}=\mathbf{p}_s-\mathbf{A}_s$ yields the following connection between the scattering angle φ at the instant of rescattering and the observed scattering angle θ:

$$\cot\theta=\cot\varphi-\frac{A_s}{|\mathbf{k}_s+\mathbf{A}_s|\sin\varphi}. \tag{34}$$

Analogously, we can express the angle φ through the angle θ by the relation

$$\tan\varphi=\frac{p\sin\theta}{p\cos\theta+A_s}. \tag{35}$$

Both the angle θ and the angle φ are defined in the laboratory system. However, the scattering angle θ_s in Eqs. (31) and (32) is defined in the scattering system whose z axis is defined by the vector $\mathbf{k}_s+\mathbf{A}_s$, which can be in the direction of the polarization axis of the laser field (in this case we have $k_s+A_s>0$ and $\theta_s=\varphi$) or in the opposite direction ($k_s+A_s<0$ and $\theta_s=\varphi-\pi$; we consider the angles in the counterclockwise direction as positive—see Fig. 1).

The incident electron momentum in the laser field just before the elastic rescattering at the time $\tau_s'=\mathrm{Re}\,\tau_{s_1}=\mathrm{Re}\,\tau_{s_2}$ is $\mathbf{k}_s+\mathbf{A}_s$ and the corresponding electron kinetic energy is $E_s=(\mathbf{k}_s+\mathbf{A}_s)^2/2=p_s^2/2$. In Refs. [24–27] it was estimated that $p_s=1.26A_s$ using the classical result that the maximal energy of the returning electron is $3.17U_p$ ([38–40]; see also Sec. III in the review article [2]; for the few-cycle laser-pulse case, see [4]). Also, it was supposed that $E_s=3.17U_p^{\mathrm{eff}}$, with $U_p^{\mathrm{eff}}=A_s^2/4$. Having developed our quantum-orbit theory, we are able to give a better estimate of this energy. In principle,

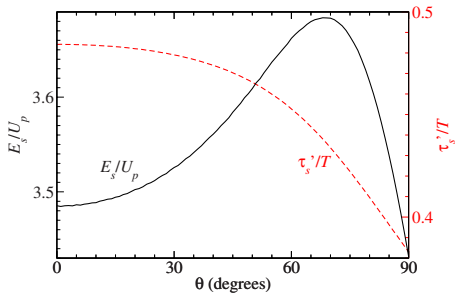

FIG. 2. (Color online) Maximal electron kinetic energy E_s at the time of rescattering (left ordinate—black solid line) and the corresponding rescattering time τ_s' (right-hand ordinate—red dashed line) as functions of the scattering angle θ. HATI of Xe atoms by the laser field having the intensity 1.5×10^{14} W/cm^2 and the wavelength 760 nm is considered.

the energy E_s and the vector potential $A_s\equiv A(\tau_s)$ depend on the scattering angle θ. This is shown in Fig. 2 for the parameters of the above-mentioned Xe example. The maximum energy slowly increases from $3.48U_p$ for $\theta=0°$ up to a maximum $3.68U_p$ for $\theta=68°$ and then decreases to $3.43U_p$ at $\theta=90°$ (for an infinitely long pulse the symmetry upon $\theta\leftrightarrow180°\pm\theta$ is valid, so that we present only the results for $0°\le\theta\le90°$) [41]. The rescattering time starts slightly below $T/2$ (T is the period of the laser field) and slowly decreases with the increase of θ.

Let us denote $A_r\equiv A_s(\theta=0)$ and draw a semicircle in the (p_z,p_x) plane with radius $p_r=|p_{\max}(\theta=0)+A_r|$ and center located at $-\mathbf{A}_r$. The angle θ_r changes from $-180°$ to $0°$ (this case corresponds to the upper panel of Fig. 1). From Fig. 3 we see that this semicircle for large scattering angles agrees very well with the blue (solid) curve $(p_{\max}(\theta)\cos\theta, p_{\max}(\theta)\sin\theta)$, where $p_{\max}^2(\theta)/2=E_{\mathbf{p},\max}(\theta;\beta m=-10)$ is obtained solving the system of the saddle-point equations. In this context, the simple analytical formula [37]

$$E_{\mathbf{p},\max}(\theta=0)=10.007U_p-0.538E_i$$

and

$$A_r/A_0=\cos\omega\tau_r'\approx-1 \tag{36}$$

can be used as a good approximation.

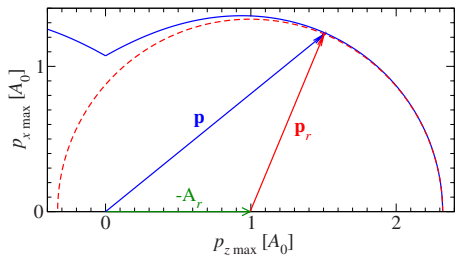

FIG. 3. (Color online) Maximal photoelectron momenta presented in the (p_z,p_x) plane. Blue (solid) line: results for the drift momentum $\mathbf{p}$ obtained using the saddle-point method. Green line: vector potential $\mathbf{A}_r$ at the rescattering time which corresponds to the maximal drift electron energy for scattering angle $\theta=0$. Red dashed line (semicircle) is determined by the vector $\mathbf{p}_r$, defined in the text.

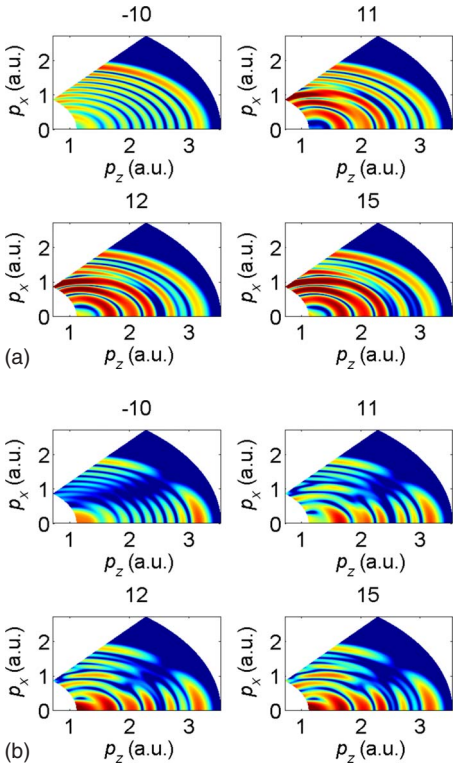

FIG. 4. (Color online) Ionization rates of Ar presented in false colors in the (p_z,p_x) momentum plane. The laser intensity and wavelength are 2.3×10^{14} W/cm^2 and 800 nm, respectively. The upper (lower) four panels are obtained using the first Born approximation (low-frequency approximation) for the rescattering matrix element. Each panel is denoted by the maximum number βm used in the sum over the saddle-point solutions in the uniform approximation.

It is well known that many more saddle-point solutions contribute and that their interference gives complicated spectra ([20,23] and references therein) and, for long pulses, leads to resonantlike enhancements [21,22]. Even in the cutoff region two solutions contribute. Nevertheless, as we have mentioned in Sec. I, the simple factorization formula (31) works well and is in accordance with the experiments [27,28]. It should also be mentioned that our definition of the cutoff as the approaching point of the solutions s_1 and s_2 is slightly beyond the point of the maximal yield. This means that our cutoff corresponds to the outer semicircle of the BRR.

III. NUMERICAL RESULTS

We calculate the ionization rates using the uniform approximation as described in Sec. IID of Ref. [21]. In Figs. 4 and 5 the ionization rates (in atomic units) of Ar ($E_i=-15.76$ eV) by a laser field having the wavelength 800 nm and the intensity 2.3×10^{14} W/cm^2 are presented in false colors in the (p_z,p_x) plane or in the $(\theta,E_\mathbf{p})$ plane. The scale is $\log_{10}$ and the color bar (not shown) covers the range from −4 to −2, i.e., 2 orders of magnitude. All values below and above this range are set equal to the limits −4 and −2,

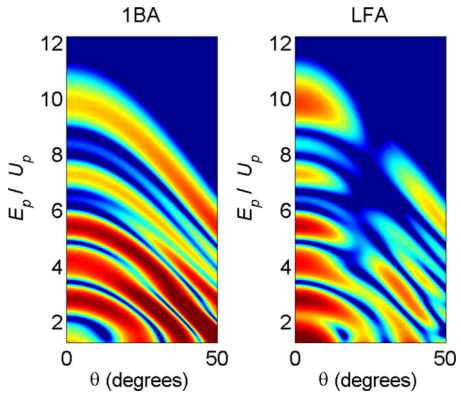

FIG. 5. (Color online) Ionization rates of Ar presented in false colors in the electron emission angle-energy plane. The final electron energy is in units of the ponderomotive energy U_p. The laser parameters are as in Fig. 4. Ten pairs of quantum orbits are taken into account. The left (right) panel corresponds to the results obtained using the first Born approximation (low-frequency approximation) for the rescattering matrix element.

respectively. The angle θ changes from 0° to 50°. The energy starts slightly above the ionization energy $-E_i$ and goes beyond the cutoff for the corresponding angle θ. In the uniform approximation the pairs of orbits having $\alpha=-1$ and $\alpha=+1$ are unified. Figure 4 shows the rates in the momentum plane. The upper left panel presents the rates obtained using only the pair $\alpha=\pm1$ with $\beta=-1$ and $m=0$ (see Fig. 1 in [21] for the classification of orbits). This is the pair of orbits with the shortest "travel time," which is the time between ionization and rescattering. This result is labeled by $\beta m=-10$. The upper right panel in addition includes the contribution of the pair $(\alpha=\pm1)$ of the two next-to-shortest orbits, which in our nomenclature are labeled by $\beta m=11$. Note that the contributions of the pair $\beta m=11$ *are not displayed separately but added* with their proper phases as demanded by Eq. (29) to those of the shortest pair $\beta m=-10$. This panel is labeled by 11. The next panel in row, identified by $\beta m=12$, includes the contributions of the four pairs: $\beta m=\{-10,11,-11,12\}$. Finally, the panel labeled $\beta m=15$ includes the ten pairs that are listed in Table I whose last member is 15. The results presented in Fig. 5 in the angle-energy plane include contributions of these ten pairs. The upper four panels of Fig. 4 are obtained using the 1BA for the rescattering matrix element, while the lower four panels are based on the LFA, which takes into account the exact elastic rescattering amplitude. Figure 5 presents the same data in the angle-energy plane, but only the results corresponding to the panels 15 of Fig. 4 are shown.

Comparison of the upper and the lower panels of Fig. 4 shows that the 1BA can be used only for small angles (say below 10°), while for larger angles the results are qualitatively different due to the different behavior (the appearance of minima) of the differential cross section of the particular inert gas (argon in our case).

In Refs. [27,28] the differential cross section for electron-ion scattering was extracted from the BRR observed in the HATI spectra. Our concept of quantum orbits allows us, in principle, to extract such data not only for the electron en-

TABLE I. Cutoff energies in units of the ponderomotive energy $U_p=13.74$ eV for the angle $\theta=0$ and for pairs of quantum orbits having the denoted values of the numbers βm. The fourth line gives the cutoff momentum along the laser polarization direction in atomic units for $U_p=13.74$ eV for comparison to Fig. 4. The laser and atomic parameters are as in Fig. 4.

βm	−10	11	−11	12	−12	13	−13	14	−14	15
E_s/U_p	3.48	1.42	2.51	1.66	2.31	1.76	2.22	1.82	2.17	1.85
$E_{\mathbf{p}}/U_p$	10.60	6.79	8.97	7.31	8.60	7.52	8.44	7.63	8.34	7.70
p_z(a.u.)	3.27	2.62	3.01	2.72	2.95	2.76	2.92	2.78	2.90	2.79

ergy which corresponds to the cutoff of the whole spectrum but also for the various lower energies that correspond to the cutoffs of particular pairs of quantum orbits. Namely, the second line of Table I shows that the cutoffs of the energy of the rescattering electron come to lie in the range $1.42U_p \leq E_s \leq 3.48U_p$ and accumulate around $2U_p$. Unfortunately, in momentum space this energy range is mapped on the narrow interval $2.62 \leq p_z(\text{a.u.}) \leq 3.27$ for the intensity corresponding to $U_p=13.74$ eV (cf. the fourth line of Table I). Hence, the analysis of the data will better be carried out in the energy-angle presentation (cf. Fig. 5). However, there is a principal obstacle that impedes the extraction of cross sections from the observed HATI data: all rescattering ridges below the BRR receive contributions from several pairs of orbits, not just the one pair $\beta m=-10$ with the shortest travel times, which contributes along the BRR. Table I shows that this is the case for rescattering energies below $E_{\mathbf{p}} \approx 9U_p$. This spoils the factorization property (1) or (31) on which the simple extraction of the elastic cross section relies. If, however, for whatever reason one pair of orbits should still dominate the rescattering rate, then the factorization (31) will hold again approximately for the corresponding pair of solutions [denoted by s in Eq. (31)]. Inspection of Fig. 4 suggests that this might be the case near the cutoff of the pair +11 of the next-to-shortest orbits and possibly also for the pair −11.

Figure 6 exhibits the results of such an analysis for the extraction of the electron-ion cross section and a comparison to a theoretical calculation. Here, for $U_p=13.74$ eV, the LFA results obtained from the shortest ten pairs of orbits as presented in the lowest right panel (15) of Fig. 4 were used to substitute an experimentally measured ionization rate (dashed red lines). The exact theoretical cross section was calculated using the method described in Appendix B (solid black lines). For the electron energies E_s at the detector that correspond to the cutoffs of the various pairs (cf. Fig. 4 and Table I) the factorization property (31) was assumed to hold, with the saddle-point solution s corresponding to the respective pair of orbits. We notice that as expected the agreement between the "experiment" and the exact theoretical calculation is very good for the highest cutoff energy of 47.8 eV, which is generated by the pair −10. This is because at the cutoff energy there is no competing pair that contributes so that the factorization property (31) holds almost exactly. For the cutoff energies of the two next-to-shortest pairs (19.5 eV for the pair +11 and 34.5 eV for the pair −11) the agreement is still reasonable for angles not too far away from the polarization axis. The contributions of longer and longer pairs of orbits accumulate near the energy of ≈27.5 eV. It is therefore not surprising that in this region the approximation by one single pair fares most poorly. This is, in fact, borne out by the remaining panels of Fig. 6.

The reliability of this method of extraction is likely also to depend on the laser intensity. Therefore, in Fig. 7 we present the results of the same analysis for several different laser intensities, this time only for the three pairs of shortest orbits −10, +11, and −11. Again, for all four intensities considered, $I=[1,1.5,3,3.5]\times 10^{14}$ W/cm^2, the agreement between the extracted cross section and its theoretical calculation along the lines of Appendix B is excellent at the cutoff energy of the BRR where the pair of orbits $\beta m=-10$ is the only one to contribute. It becomes worse for subsequent cutoff energies corresponding to the pairs $\beta m=+11$ and $\beta m=-11$.

The problem that stands in the way of extracting cross sections for various energies of the incident electron out of HATI data at one fixed intensity is the fact that more than one pair of quantum orbits contributes to the angle-resolved spectrum, with the sole exception of the spectrum along and beyond the BRR where only the shortest pair of orbits plays a role. However, as a theoretical consistency check of our formalism, we may suppress the contributions of all pairs of orbits from the rate (29) but for the one that has its cutoff at

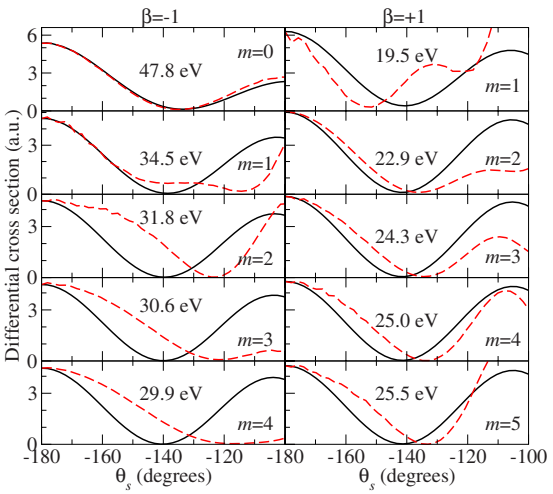

FIG. 6. (Color online) Angular distributions of the differential cross sections for elastic scattering of electrons on Ar ions (black solid curves). The electron kinetic energies given in the various panels correspond to the incident energies E_s which, after the electron rescattering and propagation in the laser field, lead to the final electron energy at the detector equal to the cutoff energy of the corresponding pair βm of quantum orbits. Red dashed curves correspond to the results extracted from the HATI spectra of Fig. 4 (lowest right panel, LFA with ten pairs of orbits) for the same laser parameters as in Fig. 4.

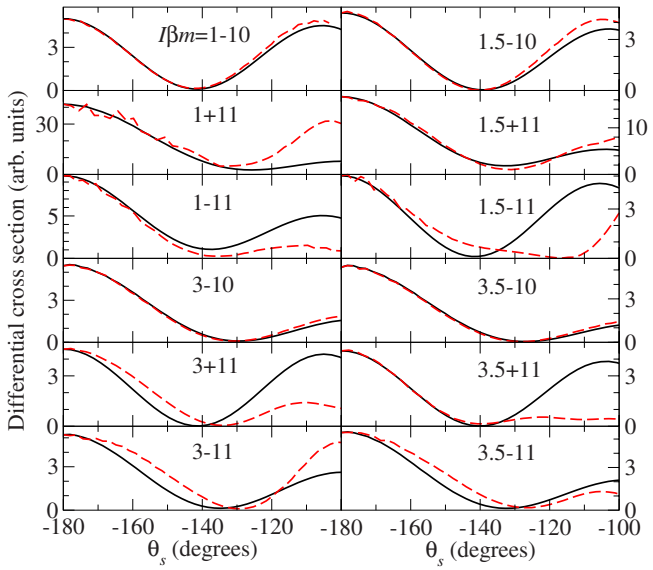

FIG. 7. (Color online) Angular distributions of the differential cross sections for elastic scattering of electrons on Ar ions (black solid curves). The electron kinetic energies used in the various panels correspond to the incident energies E_s which, after the electron rescattering and propagation in the laser field, lead to the final electron energy at the detector equal to the cutoff energy of the denoted pair βm of quantum orbits. Red dashed curves correspond to the results extracted from the HATI spectra obtained using LFA with nine pairs of orbits. The laser wavelength is 800 nm and the intensity I is 1, 1.5, 3, and 3.5 in units of 10^{14} W/cm^2, as denoted in each panel.

the energy in question and employ the results as a new "experiment." Such an example is presented in Fig. 8 for the same Ar example as in Figs. 4 and 5. Each panel of Fig. 8 corresponds to specific values of the quantum-orbit numbers βm and of the incident electron energy just before rescattering. The corresponding cutoff energies are tabulated in Table I. The theoretical results (black solid lines) are the same as in

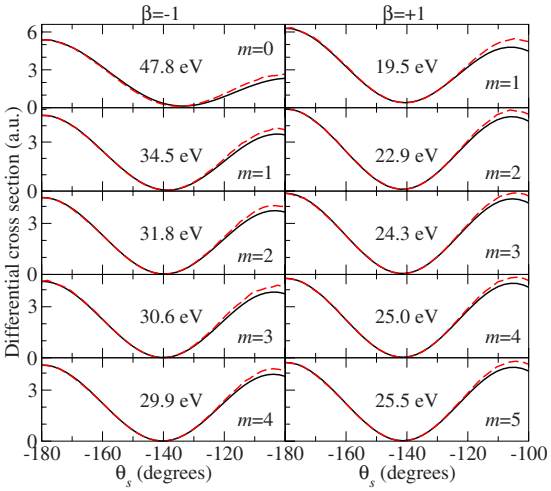

FIG. 8. (Color online) Same as in Fig. 6 except that the HATI spectra, from which the data presented by the red dashed curve were extracted, were calculated taking into account only the pair βm of quantum orbits, as explained in the text.

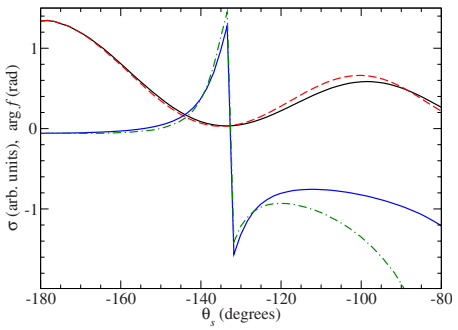

FIG. 9. (Color online) Angular distributions of the differential cross section [black solid curve $\sigma(p_s,\theta_s)$] and the phase of the scattering amplitude [blue solid curve arg $f(p_s,\theta_s)$] for elastic scattering of electrons on Ar ions. Red dashed curve and green dot-dashed curve correspond to the cross section and the phase extracted from the HATI spectra along the BRR for the same laser parameters as in Fig. 4.

Fig. 6. Now the agreement between the cross section extracted from the "experiment" and the theoretical calculation is excellent, but we remind the reader that this was a consistency check only and not a viable method of how to obtain electron-ion cross sections at various energies from experimental HATI spectra at one fixed laser intensity.

As a final consistency check, we will also scrutinize the phase relation (33). Like before, this does not allow one to extract the phase of the scattering amplitude from experimental data, since the phase arg $T_{\mathbf{p}i}^{\mathrm{BRR}}(n)$ is not experimentally accessible. We restrict ourselves to the BRR. For the laser parameters as in Fig. 4, the maximal electron kinetic energy $p_s^2/2$ at the time of rescattering continuously increases from 47.8 eV for $\theta_s=-180°$ ($\theta=0°$) to 48.6 eV for $\theta_s=-100°$ and then decreases to 47.8 eV for $\theta_s=-80°$. Like the corresponding exact scattering cross section, the phase of the scattering amplitude is calculated using the results of Appendix B (solid lines). In Fig. 9 we compare this phase to the results extracted from the HATI spectra along the BRR. The agreement is very good. We notice that the phase of the scattering amplitude changes by π when the scattering angle goes from below to above the zero of the scattering amplitude, which is located at about $-132°$.

IV. CONCLUSIONS AND PERSPECTIVES

We have derived the low-frequency approximation for the rescattering T-matrix element which describes the high-order above-threshold ionization process. This result goes beyond the known improved strong-field approximation in the sense that it replaces the first-order Born approximation for the elastic rescattering amplitude with the exact scattering amplitude taken on the energy shell. Since the exact scattering amplitude has minima for particular values of the scattering angle, the difference between the angle-resolved ISFA and LFA HATI spectra becomes especially noticeable for larger angles (see Fig. 5).

Using our quantum-orbit theory and the uniform approximation we have derived a factorization formula for the rescattering matrix element. This formula enables us to deter-

mine the angular dependence of the differential cross section of the laser-free scattering amplitude from the angle-resolved HATI spectra. It can be used in those regions of momentum (or energy-angle) space where one pair of orbits dominates the result. The highest cutoffs are along the BRR and they are well separated from the cutoffs of other pairs so that the influence and possible interference of longer-quantum-orbit contributions are negligible and the angular dependence of the corresponding laser-free elastic differential cross sections can be extracted from the measured HATI spectra to excellent accuracy [27,28]. We have shown in Figs. 6 and 7 that a corresponding analysis can still be applied for energies near the cutoffs of the next two pairs of orbits (ordered by increasing length of the travel time), but the procedure becomes less accurate and only works sufficiently close to the laser polarization axis.

It is known that a multiplateau structure in HATI spectra develops for an elliptically polarized laser field [42–44]. The cutoff regions of these plateaus each only receive contributions from one pair of orbits. Following the BRRs that correspond to each of these plateaus one can therefore extract the laser-free differential cross sections for each of these energies from just one measurement of the angle-resolved HATI spectra (in analogy with Fig. 8). Unfortunately, the phase of the scattering amplitude cannot be determined in such a measurement. However, for few-cycle laser pulses, recording the angle-resolved spectra for different carrier-envelope phases, this may become possible. The situation is further simplified by the fact that in this case a smaller number of quantum orbits contribute [45]. Another possibility is to use a bichromatic laser field and to record data for different values of the relative phase between the field components [46].

The theory presented in this paper can be generalized to molecular HATI. The improved SFA has already been developed for molecular HATI [11]. The first simulation of the experiments using this theory was successful [47]. We expect that the details of the angle-resolved spectra can be better reproduced using the molecular LFA theory which we are planning to develop.

ACKNOWLEDGMENTS

We enjoyed discussions with Anh-Thu Le, C. D. Lin, and T. Morishita. Support by the VolkswagenStiftung and by the Federal Ministry of Education and Science, Bosnia and Herzegovina is gratefully acknowledged.

APPENDIX A: DERIVATION OF EQ. (19)

The total time-evolution operator $U(t,\tau')$ in Eq. (15) propagates the laser-field-free state $\psi_{\mathbf{p}}(t)$ back to the state $\phi_{\mathbf{p}}(\tau')$ in the presence of the field, which is the solution of the Schrödinger equation with the total Hamiltonian $H(\tau')$. It satisfies the Lippman–Schwinger equation

$$|\phi_{\mathbf{p}}(t)\rangle = |\chi_{\mathbf{p}}(t)\rangle + \int_{-\infty}^{\infty} dt' G(t,t') V(\mathbf{r}) |\chi_{\mathbf{p}}(t')\rangle, \quad \text{(A1)}$$

where $G(t,t') \equiv G^{(+)}(t,t') \equiv -iU(t,t')$ for $t > t'$, $G^{(+)}(t,t') = 0$ for $t < t'$, is the total retarded Green's operator. This allows us to rewrite the scattering matrix element in Eq. (15) in the form

$$M_{\mathbf{pk}}(t,\tau) = -i \int_{\tau}^{t} d\tau' \int_{-\infty}^{\tau'} dt' \langle \chi_{\mathbf{p}}(t') | [\delta(t'-\tau') + V G^{(-)}(t',\tau')] V | \chi_{\mathbf{k}}(\tau') \rangle. \quad \text{(A2)}$$

Next, we formally expand the Green's operator in powers of the stationary Green's operator $G_V(E) = (E + i\varepsilon - H_V)^{-1}$, defined in Eq. (21), by adding and subtracting the c number E in the total Hamiltonian $H(t)$,

$$\begin{aligned} G(t,t') &= \left[i\frac{\partial}{\partial t} - H(t) \right]^{-1} \delta(t-t') \\ &= \left[i\frac{\partial}{\partial t} - H_V - \mathbf{r}\cdot\mathbf{E}(t) + E - E \right]^{-1} \delta(t-t') \\ &= \{(E - H_V + i\varepsilon)\{1 - (E - H_V + i\varepsilon)^{-1} \\ &\quad \times [\mathbf{r}\cdot\mathbf{E}(t) + E - i\partial_t]\}\}^{-1} \delta(t-t') \\ &= \sum_{n=0}^{\infty} \left\{ G_V(E) \left[E + \mathbf{r}\cdot\mathbf{E}(t) - i\frac{\partial}{\partial t} \right] \right\}^n G_V(E)\, \delta(t-t'). \end{aligned} \quad \text{(A3)}$$

We will choose

$$E = \frac{1}{2}[\mathbf{p} + \mathbf{A}(t)]^2 \equiv E_{\mathbf{p}+\mathbf{A}(t)}. \quad \text{(A4)}$$

Owing to the identity

$$\begin{aligned} i\frac{\partial}{\partial t} |\chi_{\mathbf{p}}(t)\rangle &= i\frac{\partial}{\partial t} \{ e^{i\mathbf{r}\cdot\mathbf{A}(t)} |\mathbf{p}\rangle \exp[-iS_{\mathbf{p}}(t)] \} \\ &= [\mathbf{r}\cdot\mathbf{E}(t) + E_{\mathbf{p}+\mathbf{A}(t)}] |\chi_{\mathbf{p}}(t)\rangle, \end{aligned} \quad \text{(A5)}$$

this will allow us to drop all terms in the expansion (A3) with $n \geq 1$. This yields the expression (19) in the main body of the paper.

Such approximation was called the off-shell LFA in Refs. [33,34] since, in general, $[\mathbf{p}+\mathbf{A}(\tau')]^2/2 \neq [\mathbf{k}+\mathbf{A}(\tau')]^2/2$ and the T-matrix element $\langle \mathbf{p}+\mathbf{A}(\tau') | T_V(E_{\mathbf{p}+\mathbf{A}(\tau')}) | \mathbf{k}+\mathbf{A}(\tau') \rangle$ is taken off the energy shell. An explicit derivation and the range of validity of the off-shell LFA for arbitrary gauge and laser polarization were given in [34] (see also Appendix A in [33]). Therefore, the amplitude for the laser-assisted scattering in the first Born approximation, Eq. (18), should be replaced by the off-shell LFA laser-assisted scattering amplitude

$$\mathcal{M}_{\mathbf{pk}}^{\mathrm{LFA}}(\tau') = -i \langle \psi_{\mathbf{p}+\mathbf{A}(\tau')} | V(\mathbf{r}) | \mathbf{k} + \mathbf{A}(\tau') \rangle e^{iS_{\mathbf{p}}(\tau') - iS_{\mathbf{k}}(\tau')}. \quad \text{(A6)}$$

APPENDIX B: SCATTERING AMPLITUDE

In this appendix we describe our method of calculation of the scattering amplitude in the absence of the laser field. We want to calculate the matrix element $\langle \boldsymbol{k}_f | V | \psi_{\boldsymbol{k}_i}^{(+)} \rangle$, i.e., the scattering amplitude

$$f = -(2\pi)^2 \langle \boldsymbol{k}_f | V | \psi_{\boldsymbol{k}_i}^{(+)} \rangle, \tag{B1}$$

where $V=V(r)$ is a spherically symmetric short-range potential, $|\boldsymbol{k}_f\rangle$ is the plane wave corresponding to the final momentum $\boldsymbol{k}_f$, and $|\psi_{\boldsymbol{k}_i}^{(+)}\rangle$ is the stationary scattering wave. Assuming that the scattering is elastic ($k_f=k_i=k$) and using the method of partial waves, we obtain the following expression for the scattering amplitude [48]:

$$f(k,\theta) = \frac{1}{k}\sum_{l=0}^{\infty} (2l+1)\exp[i\delta_l(k)]\sin\,\delta_l(k) P_l(\cos\,\theta), \tag{B2}$$

where l is the orbital angular-momentum quantum number, $\delta_l(k)$ are the phase shifts for the given values of the quantum number l and the momentum k, θ is the scattering angle, and P_l are the Legendre polynomials. In order to obtain the phase shifts δ_l, we solve the radial Schrödinger equation

$$\left[\frac{d^2}{dr^2} - \frac{l(l+1)}{r^2} - 2V(r) + k^2\right] u_l(k,r) = 0. \tag{B3}$$

The asymptotic behavior of the function $u_l(k,r)$ is given by

$$\lim_{r\to\infty} u_l(\rho) = A_l j_l(\rho) - B_l n_l(\rho), \tag{B4}$$

where $j_l(\rho)$ and $n_l(\rho)$ are regular and irregular Ricatti-Bessel functions, respectively, and $\rho=kr$. We integrate the radial Schrödinger equation (B3) from $r=0$ to $r=a$, where a is chosen large enough for the asymptotic form (B4) to be valid. The phase shifts are determined by the formula

$$\tan\,\delta_l(k) = \frac{kj_l'(ka) - \alpha_l(k) j_l(ka)}{kn_l'(ka) - \alpha_l(k) n_l(ka)}, \tag{B5}$$

where $j_l'(ka)=[dj_l(\rho)/d\rho]_{\rho=ka}$ and $n_l'(ka)=[dn_l(\rho)/d\rho]_{\rho=ka}$, while the logarithmic derivative

$$\alpha_l(k) = [u_l^{-1}(du_l/dr)]_{r=a} \tag{B6}$$

is obtained after a numerical integration of the radial Schrödinger equation (B3) has yielded the wave function $u_l(k,r)$ and its first derivative at $r=a$.

We consider now the situation where the Coulomb interaction V_C is added to the short-range potential V_S, i.e.,

$$V(r) = V_S(r) + V_C(r), \quad V_C(r) = -\frac{Z}{r}. \tag{B7}$$

In this case, the scattering amplitude is

$$f(k,\theta) = f_C(k,\theta) + \hat{f}(k,\theta), \tag{B8}$$

where

$$f_C(k,\theta) = -\gamma \exp(2i\sigma_0)\frac{\exp\{-i\gamma \log[\sin^2(\theta/2)]\}}{2k\,\sin^2(\theta/2)} \tag{B9}$$

is the Coulomb scattering amplitude with $\gamma=-Z/k$ and $\sigma_0=\arg\,\Gamma(1+i\gamma)$, while

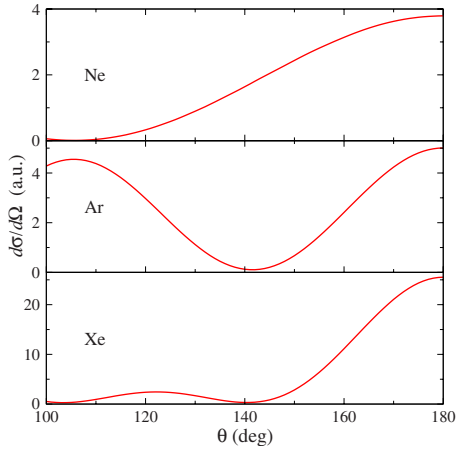

FIG. 10. (Color online) Angular distributions of differential cross sections for elastic scattering of electrons on Ne, Ar, and Xe ions. The electron kinetic energies are 39, 23, and 16.5 eV for Ne, Ar, and Xe ions, respectively.

$$\hat{f}(k,\theta) = \frac{1}{k}\sum_{l=0}^{\infty} (2l+1)\exp[2i\sigma_l(k)]\exp[i\hat{\delta}_l(k)] \times \sin\,\hat{\delta}_l(k) P_l(\cos\,\theta) \tag{B10}$$

is the additional scattering amplitude due to the existence of the short-range potential V_S in the presence of the Coulomb field V_C. In the above equation, $\sigma_l(k)$ are the Coulomb phase shifts and $\hat{\delta}_l(k)$ are the additional phase shifts due to the existence of the short-range potential V_S in the presence of the Coulomb field V_C. Note that the phase shifts $\hat{\delta}_l(k)$ are not the same as the phase shifts $\delta_l(k)$ which would be obtained from V_S alone. The Coulomb phase shifts $\sigma_l(k)$ are given by

$$\sigma_l(k) = \arg\,\Gamma(l+1+i\gamma), \tag{B11}$$

while the phase shifts $\hat{\delta}_l(k)$ can be calculated solving the radial Schrödinger equation (B3) with $V(r)=V_S(r)+V_C(r)$. The asymptotic form of the solution of this equation and the expression for $\tan\,\hat{\delta}_l(k)$ are analogous to those given by Eqs. (B4)–(B6) but with the functions j_l and n_l replaced by the regular and irregular spherical Coulomb functions F_l and G_l [48,49].

In the case of electron-atom or electron-ion scattering, a possible form of the scattering potential is [50]

$$V(r) = -\frac{Z + a_1 e^{-a_2 r} + a_3 r e^{-a_4 r} + a_5 e^{-a_6 r}}{r}, \tag{B12}$$

where Z is the charge seen by the incoming electron asymptotically. The first term in Eq. (B12) is the Coulomb potential $V_C(r)=-Z/r$. As the Coulomb field has an infinite range, we may replace it with a "screened" Coulomb potential. A possible choice is the potential [48] $V_{\rm scr}(r)=V_C(r)\exp(-r/R_s)$, where R_s is the screening distance. Another choice is [51]

$$V_{\rm scr}(r) = \begin{cases} V_C(r), & r < R_s \\ V_C(r) - V_C(r)\tanh[(r-R_s)/10], & r \geq R_s. \end{cases} \tag{B13}$$

The detachment of electrons from negative ions can also be considered using our method. In this case, the form of the electron-atom scattering potential is given in [19,26].

Finally, we present an example of our calculation of the differential cross section for elastic electron-ion scattering. In Fig. 10 we show the angular distributions of the differential cross sections for elastic scattering of electrons on Ne, Ar, and Xe positive ions. Our results agree very well with those presented in Fig. 3 in Ref. [27].

[1] L. F. DiMauro and P. Agostini, Adv. At., Mol., Opt. Phys. **35**, 79 (1995).

[2] W. Becker, F. Grasbon, R. Kopold, D. B. Milošević, G. G. Paulus, and H. Walther, Adv. At., Mol., Opt. Phys. **48**, 35 (2002).

[3] D. B. Milošević and F. Ehlotzky, Adv. At., Mol., Opt. Phys. **49**, 373 (2003).

[4] D. B. Milošević, G. G. Paulus, D. Bauer, and W. Becker, J. Phys. B **39**, R203 (2006).

[5] P. Agostini and L. F. DiMauro, Rep. Prog. Phys. **67**, 813 (2004); **67**, 1673 (2004).

[6] A. Scrinzi, M. Yu. Ivanov, R. Kienberger, and D. M. Villeneuve, J. Phys. B **39**, R1 (2006).

[7] H. Niikura and P. B. Corkum, Adv. At., Mol., Opt. Phys. **54**, 511 (2006).

[8] H. Niikura, F. Légaré, R. Hasbani, A. D. Bandrauk, M. Yu. Ivanov, D. M. Villeneuve, and P. B. Corkum, Nature (London) **417**, 917 (2002).

[9] T. Zuo, A. D. Bandrauk, and P. B. Corkum, Chem. Phys. Lett. **259**, 313 (1996).

[10] M. Spanner, O. Smirnova, P. B. Corkum, and M. Yu. Ivanov, J. Phys. B **37**, L243 (2004); S. N. Yurchenko, S. Patchkovskii, I. V. Litvinyuk, P. B. Corkum, and G. L. Yudin, Phys. Rev. Lett. **93**, 223003 (2004).

[11] M. Busuladžić, A. Gazibegović-Busuladžić, D. B. Milošević, and W. Becker, Phys. Rev. Lett. **100**, 203003 (2008); Phys. Rev. A **78**, 033412 (2008).

[12] M. Meckel, D. Comtois, D. Zeidler, A. Staudte, D. Pavičić, H. C. Bandulet, H. Pépin, J. C. Kieffer, R. Dörner, D. M. Villeneuve, and P. B. Corkum, Science **320**, 1478 (2008).

[13] M. Lein, J. Phys. B **40**, R135 (2007).

[14] L. V. Keldysh, Zh. Eksp. Teor. Fiz. **47**, 1945 (1964) [Sov. Phys. JETP **20**, 1307 (1965)]; F. H. M. Faisal, J. Phys. B **6**, L89 (1973); H. R. Reiss, Phys. Rev. A **22**, 1786 (1980).

[15] W. Becker, A. Lohr, and M. Kleber, J. Phys. B **27**, L325 (1994); **28**, 1931 (1995); A. Lohr, M. Kleber, R. Kopold, and W. Becker, Phys. Rev. A **55**, R4003 (1997).

[16] M. Lewenstein, K. C. Kulander, K. J. Schafer, and P. H. Bucksbaum, Phys. Rev. A **51**, 1495 (1995).

[17] D. B. Milošević and F. Ehlotzky, Phys. Rev. A **57**, 5002 (1998); **58**, 3124 (1998); J. Phys. B **32**, 1585 (1999).

[18] S. P. Goreslavskii and S. V. Popruzhenko, Phys. Lett. A **249**, 477 (1998).

[19] D. B. Milošević, A. Gazibegović-Busuladžić, and W. Becker, Phys. Rev. A **68**, 050702(R) (2003); A. Gazibegović-Busuladžić, D. B. Milošević, and W. Becker, *ibid.* **70**, 053403 (2004).

[20] E. Hasović, M. Busuladžić, A. Gazibegović-Busuladžić, D. B. Milošević, and W. Becker, Laser Phys. **17**, 376 (2007).

[21] D. B. Milošević, E. Hasović, M. Busuladžić, A. Gazibegović-Busuladžić, and W. Becker, Phys. Rev. A **76**, 053410 (2007).

[22] D. B. Milošević, E. Hasović, S. Odžak, and W. Becker, J. Mod. Opt. **55**, 2653 (2008).

[23] E. Hasović, A. Kramo, and D. B. Milošević, Eur. Phys. J. Spec. Top. **160**, 205 (2008).

[24] Z. Chen, T. Morishita, A. T. Le, and C. D. Lin, Phys. Rev. A **76**, 043402 (2007).

[25] T. Morishita, A. T. Le, Z. Chen, and C. D. Lin, Phys. Rev. Lett. **100**, 013903 (2008); New J. Phys. **10**, 025011 (2008).

[26] X. X. Zhou, Z. Chen, T. Morishita, A. T. Le, and C. D. Lin, Phys. Rev. A **77**, 053410 (2008).

[27] M. Okunishi, T. Morishita, G. Prümper, K. Shimada, C. D. Lin, S. Watanabe, and K. Ueda, Phys. Rev. Lett. **100**, 143001 (2008).

[28] D. Ray, B. Ulrich, I. Bocharova, C. Maharjan, P. Ranitovic, B. Gramkow, M. Magrakvelidze, S. De, I. V. Litvinyuk, A. T. Le, T. Morishita, C. D. Lin, G. G. Paulus, and C. L. Cocke, Phys. Rev. Lett. **100**, 143002 (2008).

[29] F. V. Bunkin and M. V. Fedorov, Zh. Eksp. Teor. Fiz. **49**, 1215 (1965) [Sov. Phys. JETP **22**, 844 (1965)].

[30] N. M. Kroll and K. M. Watson, Phys. Rev. A **8**, 804 (1973).

[31] M. H. Mittleman, *Theory of Laser-Atom Interactions* (Plenum, New York, 1993).

[32] F. Ehlotzky, A. Jaroń, and J. Z. Kamińsky, Phys. Rep. **297**, 63 (1998).

[33] D. B. Milošević, J. Phys. B **28**, 1869 (1995).

[34] D. B. Milošević, Phys. Rev. A **53**, 619 (1996).

[35] P. S. Krstić and D. B. Milošević, J. Phys. B **20**, 3487 (1987).

[36] D. B. Milošević and P. S. Krstić, J. Phys. B **20**, 2843 (1987); **21**, L303 (1988).

[37] M. Busuladžić, A. Gazibegović-Busuladžić, and D. B. Milošević, Laser Phys. **16**, 289 (2006).

[38] P. B. Corkum, Phys. Rev. Lett. **71**, 1994 (1993).

[39] G. G. Paulus, W. Becker, W. Nicklich, and H. Walther, J. Phys. B **27**, L703 (1994); G. G. Paulus, W. Becker, and H. Walther, Phys. Rev. A **52**, 4043 (1995).

[40] D. B. Milošević and F. Ehlotzky, J. Phys. B **31**, 4149 (1998).

[41] The fact that the return energies E_s significantly exceed the classical value of $3.17U_p$ is due to the additional dependence of the cutoff on the ionization potential I_P; see, M. Lewenstein, Ph. Balcou, M. Yu. Ivanov, A. L'Huillier, and P. B. Corkum, Phys. Rev. A **49**, 2117 (1994) and Ref. [37]. Physically, the increase reflects the additional kinetic energy that the revisiting electron collects while traveling from the exit of the tunnel (the position where it entered the continuum) to the center of the binding potential (the position it effectively rescatters).

[42] R. Kopold, D. B. Milošević, and W. Becker, Phys. Rev. Lett. **84**, 3831 (2000).

[43] D. B. Milošević, J. Phys. B **33**, 2479 (2000).

[44] P. Salières, B. Carré, L. Le Déroff, F. Grasbon, G. G. Paulus,

H. Walther, R. Kopold, W. Becker, D. B. Milošević, A. Sanpera, and M. Lewenstein, Science **292**, 902 (2001).
[45] D. B. Milošević, G. G. Paulus, and W. Becker, Phys. Rev. A **71**, 061404(R) (2005).
[46] C. Figueira de Morisson Faria, D. B. Milošević, and G. G. Paulus, Phys. Rev. A **61**, 063415 (2000).
[47] M. Okunishi, R. Itaya, K. Shimada, G. Prümper, K. Ueda, M. Busuladžić, A. Gazibegović-Busuladžić, D. B. Milošević, and W. Becker, J. Phys. B **41**, 201004 (2008).
[48] C. J. Joachain, *Quantum Collision Theory*, 3rd ed. (North-Holland, Amsterdam, 1983).
[49] *Computational Atomic Physics. Electron and Positron Collisions with Atoms and Ions*, edited by K. Bartschat (Springer, Berlin, 1996).
[50] X. M. Tong and C. D. Lin, J. Phys. B **38**, 2593 (2005).
[51] Z. Chen, T. Morishita, A. T. Le, M. Wickenhauser, X. M. Tong, and C. D. Lin, Phys. Rev. A **74**, 053405 (2006).